

This is a repository copy of *Functional morphology of the jaw adductor muscles in the Canidae*.

White Rose Research Online URL for this paper:

<https://eprints.whiterose.ac.uk/id/eprint/156281/>

Version: Accepted Version

Article:

Penrose, Fay, Cox, Philip Graham orcid.org/0000-0001-9782-2358, Jeffery, Nathan et al. (1 more author) (2020) Functional morphology of the jaw adductor muscles in the Canidae. *Anatomical Record: Advances in Integrative Anatomy and Evolutionary Biology*. pp. 2878-2903. ISSN: 1932-8494

<https://doi.org/10.1002/ar.24391>

Reuse

Items deposited in White Rose Research Online are protected by copyright, with all rights reserved unless indicated otherwise. They may be downloaded and/or printed for private study, or other acts as permitted by national copyright laws. The publisher or other rights holders may allow further reproduction and re-use of the full text version. This is indicated by the licence information on the White Rose Research Online record for the item.

Takedown

If you consider content in White Rose Research Online to be in breach of UK law, please notify us by emailing eprints@whiterose.ac.uk including the URL of the record and the reason for the withdrawal request.

Title: Functional morphology of the jaw adductor muscles in the

Canidae

Authors: Fay Penrose^{1,2}, Philip G Cox^{3,4}, Graham J Kemp¹, Nathan Jeffery^{1,3}

¹Institute of Ageing and Chronic Disease, Department of Musculoskeletal Biology and the MRC, Arthritis UK Centre for Integrated Research into Musculoskeletal Ageing (CIMA), University of Liverpool, Liverpool, UK

²School of Veterinary Science, Department of Veterinary Preclinical Science, University of Liverpool, Liverpool, UK

³Department of Archaeology, University of York, York, UK

⁴Hull York Medical School, University of York, York, UK

⁵Human Anatomy Resource Centre, University of Liverpool, Liverpool, UK

Corresponding author: Fay Penrose

1 INTRODUCTION

2 That anatomical form can broadly distinguish between species is a central tenet of
3 comparative biology, reflecting interrelated differences of body mass, behaviour and
4 environmental conditions as well as of phylogenetic inheritance. However, the matching of
5 specific phenotypes, or parts thereof, to particular biomechanical functions is more
6 challenging and requires further analyses beyond that of form alone. Here we explore the
7 role of differences in cranial anatomy in the biomechanics of feeding performance among a
8 closely related, but otherwise remarkably varied, family, the Canidae.

9 The 39 extant canid species (Burgin *et al.* 2018) range in body mass from less than one
10 kilogram to in excess of 80 kg and are found on all land masses except for Antarctica
11 (Wozencraft, 1993; Macdonald & Sillero-Zubiri, 2004; Sillero-Zubiri *et al.* 2004; Nowak,
12 2005; MacDonald, 2009). As is to be expected in such a globally successful clade, they
13 inhabit a wide variety of environments, from arid desert to tropical jungles, and fulfil many
14 roles from apex predator to scavenger. There are many morphological differences that allow
15 species to be distinguished, and anatomical specialisations exist, often in the context of
16 dietary and hunting behaviours. Distinct hunting strategies are linked to particular diets, and
17 consequently canids are often categorized by trophic specialisms. Groupings include
18 species that predate small mammals, those that preferentially hunt large mammals and
19 generalists (Van Valkenburgh and Koepfli 1993; Slater *et al.* 2009). All canid species are
20 opportunists and will consume carrion. Both the small prey hunters and generalist canids are
21 also known to eat varying quantities of plant material.

22 Previous studies have demonstrated the link between these trophic groups and the bony
23 morphologies of the skull. They found that the hypercarnivorous species have short broad
24 snouts, domed skulls and robust mandibles, whilst the head shapes of non-hypercarnivorous
25 canids are more gracile with somewhat flattened skulls and long slender muzzles (Van
26 Valkenburgh & Koepfli, 1993; Wroe & Milne, 2007; Slater *et al.* 2009; Goswami *et al.* 2011;
27 Meloro *et al.* 2015). The correlation of jaw shape with feeding and hunting behavior has led
28 previous authors to hypothesize that dietary adaptations have a significant influence on jaw
29 morphology, and that, in carnivorans in particular, hypercarnivorous jaws are built for
30 strength, whereas those of the small prey hunters and generalists are built for speed (Van
31 Valkenburgh & Koepfli, 1993; Andersson, 2005; Slater *et al.* 2009; Figueirido *et al.* 2011;
32 Prevosti *et al.* 2012; Meloro *et al.* 2015). The precise function of the different morphologies is
33 less well explored. Do the robust jaws of the hypercarnivores produce relatively greater bite
34 forces than the slender jaws of the small prey hunters? Or are they built for housing larger
35 teeth that are better anchored in sturdy jaws? This would give the advantage of better food
36 processing, and well-anchored teeth allow for strong pulling and tearing of carcasses, an
37 action that is commonly seen in hypercarnivorous carnivorans dismembering large prey
38 (Van Valkenburgh, 1996). Alternatively, perhaps the robust skulls of the hypercarnivores are

engineered to withstand potentially violent encounters with their large prey, or to dissipate great forces generated whilst chewing on tough materials. Shape differences in the caudal part of the skull are not as easy to align with diet. Previous analyses indicated that the differences in form of the cranial part of the skull are associated with changes in body mass and, specifically, that shape change is related to housing the jaw adductor muscles on the cranium (Penrose *et al.* 2016). Body mass related shape change is associated with the disparity in scaling between the jaw adductor muscles, which scale isometrically, and brain volume, which scales with negative allometry (Radinsky, 1981; Penrose *et al.* 2016). This does not however, preclude the possibility that there may be further functionality of cranial shape differences in addition to increasing surface area. The siting of the jaw adductor muscles on the skull, and the position of their origins and insertions may also influence bite performance. Differences in cranial and mandibular shapes may alter the relative arrangement of muscles on the skull with respect to key functional components such as the carnassial teeth, temporomandibular joint or coronoid process of the mandible, and may impact function.

The jaw adductor muscles are fundamental in producing forces that close the mandible and previous studies have estimated their physiological cross-sectional areas and force production capabilities using dry skull techniques (Wroe *et al.* 2005; Slater *et al.* 2009; Tseng & Wang, 2010; Damasceno *et al.*, 2013; Forbes-Harper *et al.* 2017). However, Taylor and Vinyard's work on primate jaw architecture (Taylor and Vinyard, 2013) established that studies using dry skull craniometric measurements to estimate muscle force production capabilities may greatly under or overestimate physiological cross-sectional areas, and that ideally, muscle architectural data should be incorporated into studies that estimate jaw muscle forces. The internal architecture of a muscle can greatly influence its functionality (Gans, 1982; Anapol & Barry, 1996; Huq *et al.* 2015; Terhune *et al.* 2015). For example, muscles with parallel fibres allow for maximum excursions and high contractile velocities, whilst muscles with internal tendons or a pennate arrangement of fibres maximize force production capability (Taylor and Vinyard, 2013). Therefore, estimations of cross-sectional areas or even directly recorded muscle masses are broad approximations of force production which may not directly translate into a pro-rata amount of force, with inequalities between mass and force contributions accounted for by the internal architecture of the muscles.

The aim of this study is to explore the form and function of the jaw adductor muscles, and to determine if differences in skull shape influence bite performance. Specifically, we test two hypotheses:

- H1 That there are significant relative, as well as absolute, differences of muscle force and bite force that reflect canid dietary niches.

This predicts for example, that hypercarnivorous species can generate larger muscle and bite forces than can small prey specialists and generalists, both in absolute terms and relative to body mass. Previous studies (Christiansen & Wroe, 2007; Damasceno *et al.* 2013) have posited and evaluated variations of this hypothesis on the basis of dry skull calculation methods.

H2 That the efficacy of muscle force production, and its conversion into bite force, is indicative of different dietary niches.

This predicts, for example, that the hypercarnivorous species are more effective at converting muscle force into bite force than any other dietary groups. Here we test the hypothesis using three key measures of performance. These are: *mechanical efficiency*, a measure of input muscle forces versus bite forces generated (Dumont *et al.* 2011; Cox *et al.* 2012); *mechanical advantage*, considered here in terms of the angle between lines of action of temporalis, the largest jaw adductor, and the occlusal plane as well as in terms of lever arm ratios (Fearnhead *et al.* 1955; Reduker, 1983); and *cranial deformation*, reflecting the amount of energy expended in deforming the skull during bite force production and typically approximated on the basis of finite element simulations of strain energy density (Dumont *et al.* 2009).

MATERIALS AND METHODS

Specimens

The dataset comprised 21 canid specimens across 12 species, representing nine of the 13 extant genera that make up the Canidae. For this study we follow the categorization of Slater *et al.* (2009): four species (*Canis lupus*, *Cuon alpinus*, *Lycaon pictus* and *Speothos venaticus*) were considered hypercarnivorous, five species were considered small prey specialists (*Alopex lagopus*, *Canis mesomelas*, *Chrysocyon brachyurus*, *Vulpes corsac*, *Vulpes vulpes*), and three considered as generalists (*Nyctereutes procyonoides*, *Otocyon megalotis*, *Vulpes zerda*). Specimens were obtained with ethical approval (University of Liverpool, Veterinary Research Ethics Committee RETH000553/VREC480) from either euthanized zoo stock or vermin control. For this study, taxonomy follows Wozencraft (1993). The sample included representatives from the three major clades (wolf-like, fox-like, South American) after Lindblad-Toh *et al.* (2005) (Table 1). The dataset is not inclusive of all canid species, but it covers a broad range of head shapes, body sizes and phylogenetic groups, and includes all four of the hypercarnivorous species (Van Valkenburgh & Koepfli, 1993). Although numbers of specimens were low for all species in this study, the diversity of scale covered two orders of magnitude, and interspecific differences were likely to predominate.

All specimens were adults, with exact ages recorded by donor organizations in six specimens, and maturity established for the others with reference to dental wear. In most cases, only the heads were available, and so mean body masses reported in the literature were used for all calculations (Table 1). Some degree of sexual dimorphism has been documented in many canid species. The literature however, concurs that any differences are very modest and that overall body size is the greatest differential factor, and that many of the largest females have a greater body mass than the smallest males (Gittleman & Valkenburgh, 1997; Macdonald & Sillero-Zubiri, 2004; Sillero-Zubiri *et al.* 2004; MacDonald, 2009; Wang & Tedford, 2010; Kim *et al.* 2012). Specimens were either chilled fresh or frozen and then defrosted, but no fixative agent was used on any specimen.

Imaging

Computed tomography (CT) was used to capture the three-dimensional architectural detail of the skull and mandible at occlusal, or near occlusal, bite. Heads were scanned at the University of Liverpool either at the Small Animal Teaching Hospital using a Siemens Somatom Volume Zoom (Siemens AG, Munich) or a Toshiba Prime Aquilion (Toshiba Medical Systems, Europe), or at the Philip Leverhulme Equine Hospital using a GE Lightspeed Plus (GE Medical Systems, Milwaukee). Pixel resolution and slice thickness varied to reflect the different sizes of the specimens. Pixel resolution ranged from 0.136 to 0.417 mm, and slice thickness from 0.3 to 1.2 mm. Current and voltages used were 200 mA and 120 kV, respectively. Pre-processing of CT DICOM file data was undertaken with ImageJ v1.45s (Schneider *et al.* 2012). One specimen, *Vulpes vulpes* 6, was also imaged using a 3T Siemens Trio (Siemens Medical Solution, Erlangen, Germany) magnetic resonance (MR) scanner at the Liverpool Magnetic Resonance Imaging Centre at the University of Liverpool. A proton density (PD) weighted sequence was used with pixel resolution of 0.42 mm, and slice thickness of 0.5 mm. This specimen was scanned at occlusion and wide gape to capture changes in the 3D geometry of the jaw adductor muscles in the intact specimen (Fig. 1A).

Landmarking

Automatic thresholding tools in Avizo Lite 9.0.1 (Thermo Fisher Scientific, Waltham, MA) were used to identify the voxels that represented the bony and dental structures of the head. These were then reconstructed to produce virtual models of each skull. Models were used to locate and place landmarks at the prosthion, the caudal end of the hard palate and the basion of the skull. This allowed measurements of skull length and hard palate length to be used in regression analyses.

Dissection methods

Differentiation of individual muscle layers is difficult to ascertain using imaging methods alone, and so specimens were dissected to determine the detailed anatomy of each muscle and its subdivisions, including their origins and insertions. One side of each cadaveric head, either left or right, was dissected. All specimens were dissected at or near dental occlusion, that is, with the jaws in the closed position. No individual was judged to have a preferential working side from inspection of dental wear. Each specimen was photographed using a digital camera (Sony DSC-H200) positioned perpendicular to the sagittal, axial and coronal planes. The temporalis, masseter and pterygoid muscles were dissected in all specimens. Muscle mass and the extent and position of origins and insertions were recorded for all muscles and their subdivisions. After the removal of the bulk of each muscle, to ensure that as much of the muscle mass as possible was recorded, any residual muscle fragments left on the bone were scraped off and added to the individual muscle masses before weighing. The temporalis was subdivided into its three constituent layers; superficial, deep and suprazygomatic. The masseter was subdivided into its three layers; superficial, deep and zygomaticomandibularis, although the division between the superficial and deep layers was often unclear, particularly in the larger species where many additional leaflets were observed. In these instances, the boundaries were determined by observing the orientation of the fascicles: the superficial muscle fascicles ran in a caudoventral orientation, whilst those of the deep masseter ran more ventrally. Medial and lateral pterygoids were treated as one muscle as the lateral pterygoid is very small in carnivores. To verify this, one specimen (*Vulpes vulpes* 7), was further dissected and the medial and lateral pterygoids were separated and their individual masses and contributions to pterygoid mass and total muscle mass determined. The action of the lateral pterygoid in the carnivorans is unclear. Some authors describe it as a jaw adductor or probable jaw adductor (Tomo *et al.*, 1995; Evans and De Lahunta, 2013; Singh *et al.*, 2018) due to the orientation of the fascicles and close association with the medial pterygoid. Others see it as a possible jaw protractor or joint stabilizer (Kawamura *et al* 1968, Turnbull 1970). All concur that its role is likely to be insignificant due to its small size and the bony constraints of the TMJ (Turnbull, 1970; Ström *et al.*, 1988; Herring, 2007; Hartstone-Rose *et al.*, 2012). Further details of the dissection protocol can be found in Penrose *et al.* (Penrose *et al.* 2016). The specimen that had undergone MR scanning at both occlusion and wide gape, *Vulpes vulpes* 6, was also subsequently dissected and photographed at occlusion and wide gape, to confirm the limit of gape (*Vulpes vulpes* 6 dissected at wide gape is shown in Fig.1b).

Gape angle at wide gape

One specimen, *Vulpes vulpes* 6, was used to determine the angle to be applied to the wide gape models in all species. This specimen was manually positioned and then secured at wide gape and imaged using MR to visualize the internal skeletal and soft tissue structures using Avizo image reconstruction software. The specimen was consequently dissected at

wide gape to confirm the angle of the mandible and the identity of the soft tissue structures, which were used to inform the accuracy of the FE models. Gape angle was measured from the caudal margin of the upper canine alveolus at the gumline to the caudal extent of the mandibular fossa of the temporal bone, and to the caudal margin of the lower most caudal molar alveolus at the level of the gumline. Wide gape angles measured in the specimen were very similar in both the MR images and dissection methods, at 84° and 81° respectively. In accordance with these measures all of the FE wide gape models were based on a gape angle of approximately 80°.

Calculating the reduced physiological cross-sectional area and force of muscle

The reduced physiological cross-sectional area (RPCSA) of each muscle was calculated using the method of Anapol and Barry after Haxton (Haxton 1944; Anapol and Barry, 1996). It uses the following equation, which, as well as muscle mass and fascicle length, also considers the effect of the pennation angles of the fascicles.

$$RPCSA = \frac{mass \times \cosine \text{ of pennation angle}}{fascicle \text{ length} \times muscle \text{ density}}$$

Muscle mass was determined using Redwag WPS600/C/2 digital scales, accurate to 0.001g. The specific muscle density value used was 1.056 gcm⁻³ based on cat soleus muscle (Murphy and Beardsley, 1974). To verify this parameter, individual volumes of the jaw adductor muscle subdivisions were predicted in two specimens, *Vulpes vulpes* 1 and *Vulpes zerda*, by dividing mass by 1.056 gcm⁻³. The volume for each muscle subdivision was then measured directly with a microvolumeter, using a method adapted by Vickerton after Douglass and Wcislo (Douglass & Wcislo, 2010; Vickerton *et al.* 2013). The two values were compared using regression analysis.

Digital photographs were analysed using the angle and measurement tools in ImageJ (Schneider *et al.* 2012). The angle of pennation for each muscle layer was measured at 5–10 locations, and fascicle length was measured at 5–20 locations, depending on the size of the muscle (Fig.2). Fascicles that had been transected during dissection were not measured. Mean values were used for calculations. Muscle force was then calculated by multiplying RPCSA by an intrinsic muscle strength value of 37 Ncm⁻² (Weijs & Hillen, 1985; Koolstra *et al.* 1988; Christiansen & Adolfssen, 2005; Christiansen & Wroe, 2007).

As many previous bite force studies have used Thomason's (1991) dry skull method to calculate cross sectional areas and muscle forces, we also used this method as a comparison to the RPCSA method (Christiansen & Adolfssen, 2005, Christiansen & Wroe, 2007; Damasceno *et al.* 2013). Authors cited here have calculated predicted bite force at

canine and/or carnassial bite points, but all at occlusal bite angle only, which we follow for this part of the study. The dry skull method uses 2D images of skulls to identify spaces that would, in life, be occupied by muscle masses. The area of each of these spaces is then used as a proxy for the cross-sectional areas of the jaw adductor muscles. In this study we identified spaces for two functional groups: the temporalis and the masseter/pterygoid mass. Whilst some authors do not distinguish between the medial and lateral pterygoid muscles (Slater *et al.*, 2009; Tseng and Wang, 2010), others nominally only include the medial pterygoid (Christiansen and Adolfssen, 2005; Christiansen and Wroe, 2007; Damasceno *et al.*, 2013; Forbes-Harper *et al.*, 2017). However, as the dry skull method includes the cross-sectional area occupied by the very small lateral pterygoids, we feel it is acceptable to include them in our calculations for this part of the study. The muscle cross-sectional areas are then multiplied by the estimated isometric force for muscle. Potential differences between calculation method results were explored using regression analyses. Regression analyses plotted muscle forces derived from both methodologies against each other to compare values. Further regression tests were carried out with muscle forces plotted against body mass for both of the data sets to determine if the muscles scaled with allometry and if the method of determining muscle force made significant differences to the result.

FE model building

A CT dataset representing one individual from each species was imported into Avizo Lite 9.0.1 for material segmentation. In species with more than the specimen, the individual closest to the mean shape was chosen based on earlier shape analysis (Penrose *et al.* 2016). Each model consisted of two main structures, the skull, and a separate region representing the caudal part of the left mandible. The mandibular region was used to locate the correct insertion points of the jaw adductor muscles and allowed us to model muscle vectors with greater accuracy. It does not form part of the final model subjected to computational simulations. Manual and automatic segmentation methods were used to identify six different materials (cortical bone, cancellous bone, teeth, nasal septum, orbital ligaments and zygomatic sutures). The teeth were treated as a single material and the periodontal ligament was not segmented but included as part of each tooth. Some architecturally intricate regions of the skull were manually removed from the models, most notably the nasal turbinate bones, the minor paranasal sinus bony subdivisions and the inner ear architecture, as these were felt to be of little relevance to the masticatory model and were likely to be computationally burdensome. Smoothing algorithms were utilized to further reduce skull complexity and thus the computational workload. The segmented models were converted to three dimensional meshes using Avizo software. Models consisted of between 994,992 and 2,483,659 tetrahedral elements. The difference in tetrahedral numbers is accounted for by the differences between the original specimen sizes and scan resolutions. In convergence tests (see Bright and Rayfield, 2011) the *Vulpes*

vulpes model solved consistently using around 300,000 elements. A factor of 3 for the minimum number of elements was introduced to account for greater morphological complexity in other species and improve acuity. In contrast with some earlier bite force studies (McHenry *et al.* 2006; Slater *et al.* 2009; Attard *et al.* 2011), we did not scale the FE models to identical volumes or loads as we had empirically derived specimen specific values for muscle forces. This approach allowed us to take into account both size and shape differences, with a view to producing more realistic functional models. Scale was set with reference to the original CT resolutions and meshes were re-orientated such that the hard palate, a relatively flat structure in canids, was parallel to the axial plane Y, rostral and caudal landmarks aligned along the sagittal plane Z, and medial and lateral structures along coronal plane X.

FE model material properties

The computational meshes were imported into PreView V1.18.2 (Maas *et al.* 2012), and the individual volumes assigned different material properties. The bony components of the skull were modelled as isotropic elastic materials with most of the skull modelled as cortical bone. We did not account for the diploë, or cancellous bone layer, in the calvarial bones as the resolution of the CT scans was too coarse. We did however model cancellous bone in areas where it was grossly evident on the CT scans, namely in the zygomatic arch, caudal cranium, rostral maxilla and premaxilla. Reported material properties of skeletal tissues are highly varied with influencing factors including species, site of bone, fresh, dried or embalmed preparation of specimens, experimental methods and age of cadaver. Studies using fresh or fresh-frozen specimens, that is, not dried or embalmed, reported lower values than those of dried specimens (Motherway *et al.* 2009; Auperrin *et al.* 2014; Falland-Cheung *et al.* 2017). As our laboratory experiments used fresh-frozen material we used a relatively low Young's modulus for cortical cranial bone. As the literature consistently suggests that cancellous bone is less stiff than that of the surrounding cortical bone, we used a lower value for cancellous bone. The only cranial suture that was modelled was the temporozygomatic suture, the oblique ventrocaudal suture between the temporal process of the zygomatic bone and the zygomatic process of the temporal bone. Inclusion of this suture in FE skeletal models has been shown to increase the performance of models, especially those investigating the masticatory apparatus (Kupczik *et al.* 2007). This is due to its close topographic association with the origin of the masseter muscle and, in canids, because it fuses either late in life (Evans and De Lahunta, 2013) or not at all (Thrall and Robertson, 2015). In all the CT scans and dissected specimens, the temporozygomatic suture could be easily perceived as a simple, rather than interdigitated, dark line, which completely separated the zygomatic and temporal bones. The temporozygomatic sutures were modelled as a neo-Hookean material to reflect their hyperplastic properties (Mohamed *et al.* 2010, Weed & Maqueda, 2010). The orbital ligaments were included because work

by Herring *et al.* (Herring *et al.* 2011) has suggested some involvement with muscle force distribution, in particular, resisting deformation of the zygomatic arches by contraction of the masseter during biting. Values of material properties from studies by other authors and the values used in this study are summarized in Table 2. A Poisson's ratio of 0.3 was used for all materials.

FE Constraints

All models were constrained at the temporomandibular joint (TMJ) in all but rotational movements around the X axis. This reflects the limited movement of carnivoran mandibles during biting where there is minimal translational or rostro-caudal movement, due to the congruent nature of the condyles and the pronounced retroarticular processes. Bilateral canine and carnassial biting were simulated by fully constraining either the tips of both upper canine teeth or the paracones of both upper carnassial teeth.

FE Loading

Muscle forces acting upon the skull were simulated by selecting nodes on the skull to represent the origin attachment sites of individual muscles. The number of nodes representing temporalis ranged from 3351 to 7630, the number of nodes for the masseter ranged from 290 to 752, and the number of nodes representing the pterygoids ranged from 510 to 1140. In the case of the temporalis and masseter each muscle origin region was subdivided into smaller regions to more accurately describe the complexities of the direction of the muscle vectors of such large muscles, and to minimize the number of vectors whose line of action would run through the interior of the cranium. The origin of the temporalis muscle was subdivided into six regions and the masseter into three regions. Due to the different muscle and skull morphology of each species, this differed slightly between individual models, and the schematic plan is illustrated in Figure 3. Muscle force was derived from the RPCSA calculations and was divided equally amongst the number of total muscle nodes to give a loading value for each node. To calculate the direction of the muscle vectors, one node from each muscle origin region on the left side of the skull was selected as the representative start node, and one node from each muscle insertion site on the left caudal mandible was selected as the representative end node (Fig 3). The locations of the start and end nodes were informed by the dissection work. In the case of the temporalis muscle, as the insertion site was so extensive, two insertion node sites were chosen, one at the dorsal part of the coronoid process for the two dorsal most subdivisions, and one more ventrally on the medial aspect of the vertical ramus of the mandible, for the remaining four subdivisions (Fig 3). Again, this aided in more accurately describing the vectors for each muscle or part muscle and minimized vectors running within the cranium. The vectors calculated on the left side were reflected to create right side sets of muscle vectors. Two

gape positions were modelled based on occlusion and maximum gape. These positions were selected in order to explore the performance of the jaw adductor muscles and skull at the extreme limits of gape. The position of the mandible at maximum gape for all species was determined with reference to the dissection of the cadaveric head and MR studies of *Vulpes vulpes* 6 (Fig.1). Digital images of dissections and MR scans at wide gape were analysed using ImageJ (Schneider *et al.* 2012) to measure the angle of the mandible relative to the rostrum. Reference points were the caudal point of the alveolus of the upper left canine, the left TMJ and the caudal point of the alveolus of the lower left most caudal molar. To simulate the wide gape position in the FE models for each species, the caudal mandibles were rotated to a similar position. The representative end nodes for each of the muscles were re-identified on the rotated mandible and their new coordinates used to recalculate the force vectors acting upon the skull. All models were solved using FEBio Preview v1.18.2 (Maas *et al.* 2012) using a quasi-static, non-linear implicit method. Solved models were explored and analysed with Postview v1.9.1. Derived outputs were rigid force, a measure of bite force, and strain energy density (SED), a measure of skull shape efficiency.

To measure the influence of shape and size on rigid force and the distribution of SED across the skull, seven midline sampling sites were identified by common landmarks on each of the FE models after Tseng and Wang (Tseng and Wang, 2010) (Fig. 3C). Midline landmarks were chosen as they were easily replicable across species and were not subject to local noise created by the constraints of the models at the TMJ and bite points. At each sampling site ten nodes were randomly chosen, and their mean value recorded. The same nodes were sampled in all four loading conditions in each model (closed canine bite, wide canine bite, closed carnassial bite, wide carnassial bite).

To compare the influence of shape only, outputs were scaled to the volume of one specimen, *Canis lupus*, after Dumont (Dumont *et al.* 2009) using the equation:

$$SE_{B'} = \left(\frac{V_B}{V_A}\right)^{1/3} \left(\frac{F_A}{F_B}\right)^2 SE_B$$

Where A is the model to which B is scaled, and B' is the newly created model. SE is strain energy, V is volume and F is force. *Canis lupus* was chosen because it is the largest canid species and so allowed us to consider any size-related performance limitations in the other species.

Mechanical efficiency

The mechanical efficiency (ME) of biting can be calculated to give an indication of the influence of skull shape on performance (Dumont *et al.* 2011). Mechanical efficiency is derived by dividing the value of the calculated predicted bite force by the total muscle force,

that is, force output divided by force input. We calculated the mechanical efficiency of all species for canine and carnassial bite, at closed and wide gape.

Mechanical advantage

A further measure of the effect of form on biomechanical function is the mechanical advantage (MA) of a muscle. Following other authors (Radinsky, 1981; Reduker, 1983; Sacco & Van Valkenburgh, 2004; Tanner *et al.* 2010; Segura & Prevosti, 2012) we calculated MA as a ratio of the length of the muscle in-lever divided by the length of the bite point out-lever. The in-lever is a line connecting the point of muscle insertion on the mandible to fulcrum, in this case the mandibular condyle. In this simplified model, the muscle insertion point for the temporalis was the dorsal coronoid process of the mandible, and for the masseter it was the ventralmost part of the angular process of the mandible. The pterygoid muscles were not included in this part of the study due to their small size. The out-levers connect the fulcrum to the bite points, that is, the tip of the lower canine and the tip of lower first molar. Longer in-levers and/or shorter out-levers increase MA and hence, increase bite force. Higher MA values are negatively correlated with transmission of velocity, and species with short jaws experience a trade-off favouring jaw closing strength over jaw closing speed (Wainwright & Richard, 1995; Preuschoft & Witzel, 2005). Measurements were made on the reconstructed CT scans using the measurement tool in Avizo, and dietary groups were compared using phylogenetic ANOVA tests and post hoc tests.

Temporalis muscle angles relative to the occlusal plane

To determine whether the muscle architecture was topographically related to the bony morphology to increase jaw closing strength or speed, we considered how the muscle line of action related to the occlusal plane. The line of action of a muscle can be calculated by drawing a line from the muscle insertion point to its origin (Jensen and Davy, 1975). The resultant line can then be measured against another, constant line, and the angle between them determined. This allows comparison between specific muscles or muscle layers, as well as between individual specimens or species. To determine the muscle lines of action using the FE models, we disregarded the parasagittal coordinates (Z), and used the X and Y coordinates to draw lines in the dorsoventral and rostrocaudal planes. To reflect the line of action of the individual muscle layers that make up temporalis we amalgamated the rostral and caudal dorsalmost areas to broadly represent superficial temporalis, the rostral, lateral and caudal areas to broadly represent the deep temporalis, with the remaining ventral area representing the suprazygomatic temporalis (Fig.3). Muscle origin points were identified as the average node coordinates for each muscle layer attachment area, and the single insertion nodes remained the same as for the FEA bite models. The line representing the occlusal plane was drawn from the lateral aspect of the alveolus of the upper canine, to the ventral aspect of the retroarticular process of the temporal bone. Phylogenetic ANOVA tests

were used to determine any differences in muscle line of action angles between the dietary groups.

Statistical analysis

In order to take account of the contribution of phylogeny to jaw adductor muscle morphology and function in the study species, statistical analyses were conducted using phylogenetic comparative methods. The phylogeny used in the analyses was pruned from a downloaded tree from Nyakatura *et al.* (2012). Differences between the dietary groups regarding the percentage contribution towards total muscle force, mechanical efficiency, SED values, mechanical advantage and temporalis lines of action were tested using phylogenetic ANOVA tests (Garland *et al.* 1993) and pairwise post hoc tests. These were performed in R (R Core Team, 2016) using the phylANOVA function of the phytools package (Revell, 2012), alongside the ape (Paradis *et al.* 2004) geiger (Harmon *et al.* 2008; Pennell *et al.* 2014) and nlme (Pinheiro *et al.* 2016) packages.

Scaling relationships between pairs of variables were determined in two ways. First, by rank correlation and reduced major axes (RMA) regression analysis and, second, by phylogenetic generalized least squares (PGLS) analysis with lambda fixed at 1. Although it is generally regarded as inappropriate to report results from both phylogenetically-independent and phylogenetic comparative methods (Freckleton, 2009), this approach is recommended in studies with a small sample size (N. Cooper pers. comm.). This is because Pagel's λ has very low power to detect phylogenetic signal in datasets of fewer than 20-30 species (Freckleton *et al.* 2002). These tests were used to determine if log transformed RPCSA and dry skull calculated muscle force values scaled against log transformed body mass to indicate isometry or allometry, and if the different calculation methods resulted in different scaling conclusions. We also tested the scaling relationships of the following variables: body mass, muscle mass, fascicle length, muscle force, bite force, rostrum length and palate length. Rank correlation and RMA regression were used as the relationships are likely to be monotonic and symmetric. Evaluations of equivalence and isometry were made based on the RMA slope, 95% confidence intervals and *P*-values from *t*-scores against predicted slope values. Rank correlation and RMA regressions were computed in PAST (Hammer *et al.*, 2001). PGLS analyses were conducted using the caper (Orme, 2012) and picante (Kembel *et al.* 2010) packages in R. Significant results are reported alongside the analyses and all results are reported in the supplementary material. A significance level of less than or equal to 0.05 was used in all statistical tests.

RESULTS.

Muscle density

Predicted and measured muscle volumes are reported in Table 3. Regression analysis found that there were no significant differences between the volume predicted from mass and that recorded by the microvolumeter (slope 0.99 from a predicted slope of 1, $r^2 = 0.99$, CI 0.98 - 1.01). This indicates that the published density value of 1.056 gcm⁻³ (Murphy and Beardsley 1974) was a reliable estimate for use in the RPCSA calculations.

Dissection, muscle mass and muscle force

Details of the muscle dissections can be found in Penrose *et al.* (2016). In a fox head dissection (*Vulpes vulpes* 7), we found that the lateral pterygoid contributed approximately 3% to the overall pterygoid mass (medial pterygoids 8.71g, lateral pterygoids 0.28g), and 0.27% to the total jaw adductor muscle mass. Of particular note is the insertion of both the deep and superficial masseter to the caudal ventral mandible. In most canid species both muscles insert on and near the angular process, but in two of the generalist species, *Otocyon megalotis* and *Nyctereutes procyonoides*, the area of insertion also extends onto the subangular process. This pronounced process is only found in a small number of canids. The dissection illustrates that the subangular process acts to change the orientation and length of the masseter fascicles (Fig. 4). The masses and fascicle lengths of the individual muscles are reported in Table 1. Regression analyses revealed that temporalis fascicle lengths were statistically proportionately significantly longer in the larger species (P -value 0.048), but that the masseter or pterygoid fascicles did not scale significantly differently from isometry. Phylogenetic ANOVA revealed that the fascicle lengths between dietary groups were statistically different for the masseter (P -value 0.04) and pterygoids (P -value 0.005), but not the temporalis. Post hoc tests revealed that for the pterygoid fascicles, the generalists were significantly different to both the hypercarnivores and the small prey specialists but could not determine which dietary groups were significantly different from one another with regard to the masseter fascicles.

Although there was some variation between species of the percentage contribution of each muscle to the overall mass, no statistically significant differences were found between the trophic groups. Similarly, the individual muscle percentage contributions towards total muscle force showed no statistical difference between trophic groups. The temporalis contributed between 44 and 61% to the total force, the masseter between 29 and 43%, and the pterygoids between 8.6 and 17%. The percentage contribution of the individual muscle masses to the total mass is not mirrored by their contribution towards the total muscle force (Fig. 5). The temporalis muscle contributed a mean value of 62% of the muscle mass, but it only contributed a mean value of 52% of the force. The masseter on the other hand, contributes a mean value 30% of the muscle mass, but a mean value of 36% of the force,

and the pterygoids contribute a mean value of 9% of the mass, but a mean value of 12% of the total force. This misalignment between mass contribution and force contribution is accounted for by the architecture of the muscles. When considering the physiological cross-sectional area, long fascicle lengths reduce the force production capability of the muscle. As the angles of pennation are small in the temporalis and masseter, typically less than 30°, they had only a small effect on the final value, as the cosine value remains close to one.

Muscle forces predicted from both the RPCSA and dry skull methods are presented in Table 1. It was noted during dissection that many of the muscle layers exhibited a great variety of pennation angles and, even more markedly, fascicle lengths. It is therefore acknowledged that the complex architecture of the masticatory muscles is difficult to capture using simple equations; however, it was felt that the RPCSA method reflects the effect of the diversity of the muscle architecture. It was noticeable that in all species over 25kg the predicted temporalis force was higher in the dry skull method than the RPCSA method, and that in all species below 14kg predicted values were lower using dry skull method than the RPCSA method. Regression analyses found that both methods for determining masseter force were well aligned (slope = 0.97, $r^2 = 0.93$, CI 0.87-1.10). When both methods of determining temporalis force values were compared, there was weak evidence of a possible skew where the dry skull method over predicts temporalis force compared to the PCSA method (slope = 1.18, $r^2 = 0.94$, CI 0.91-1.32). However, the slopes in both cases were not significantly different to 1. When muscle forces were plotted against body mass regression results from the empirically derived muscle data revealed no significant evidence for either positive or negative allometry of muscle force production capability, with slopes that are close to isometry for both the individual jaw adductor muscles and the muscle mass as a whole, when scaled against body mass (Supplementary Material). Regression results for the dry skull derived data showed that the masseter force did not scale significantly differently to isometry. The temporalis force scaled with positive allometry against body mass under an RMA model, with a slope of 0.76, but was not statistically significantly different from an expected isometric slope of 0.67 under a PGLS model. A comparison of the two slopes is shown in Fig. 6 and in Supplementary Material.

Bite forces

Predicted bite forces from the FEA models in all four loading conditions (canine and carnassial bite, occlusion and wide gape) are reported in Table 4. As expected, canine bites are weaker than carnassial bites and wide gape bites are weaker than those at occlusion.

Scaling

Spearman's rank correlation showed a statistically significant association between all pairs of variables tested (Supplementary Material). No significant allometric trends were revealed

in comparisons of bite force against body mass. The intervals and slopes for all bite forces were skewed above 0.67 under an RMA model, but not under a PGLS model. Comparisons of temporalis and pterygoid muscle force against muscle mass were also indistinguishable from isometry, whereas total muscle force against total muscle mass and masseter force against masseter mass showed weak negative allometry under a PGLS model (but not under RMA). In all cases, the scaling relationships skewed towards negative allometry in the case of temporalis and masseter, and towards positive allometry in the case of the pterygoids. When canine and carnassial occlusal bite forces were regressed against muscle forces we found that although only temporalis force vs carnassial occlusal bite was significant (P -value 0.05) (under an RMA model), all of the confidence intervals and slope values for total muscle force and temporalis force were skewed above the expected slope value for isometry (1) with values ranging from 1.13 to 1.22. This may be indicative of weak positive allometry. In contrast, under a PGLS model, the regressions of pterygoid forces with all bite forces tended towards negative allometry. Slopes from other comparisons also imply allometry, but were not sufficiently resolved to prove conclusive (see Supplementary Material).

Mechanical efficiency

Mechanical efficiency in all four conditions is reported in Table 4. Calculations found that in all species biting is most efficient toward the caudal end of the dental arcade, that is, nearer to the TMJ, and is less efficient at wide gapes. Therefore, the most efficient bite is the carnassial bite at occlusion with an average efficiency of 0.27 and the least efficient bite is the wide gape canine bite, with an average efficiency of 0.13. Phylogenetic ANOVAs revealed no statistically significant differences between trophic groups in mechanical efficiency at either of the bite points or gape angles.

FE SED models

Scatter plots of the values from the seven sample points at all four loading conditions are shown in Fig. 7. It was notable that in all species the SED values were much higher in both of the canine bite models than in either of the carnassial bite models. For example, in the largest specimen, *Canis lupus*, the greatest SED values were 3437 mJ at canine wide bite and 372 mJ at carnassial occlusal bite, and in the smallest specimen, *Vulpes zerda*, the highest SED was 646 mJ in the canine wide bite and 54 mJ in carnassial occlusal bite. During canine biting, the area of highest midline stress was at sample point 2, the level of the caudal rostrum. There was more variation in which sample site exhibited the highest SED value at carnassial bite. In most cases it was sample site 5, the bregma, but in some species, it was more rostral, at sampling sites 2, 3 or 4 (Fig. 7C and 7D). No midline sample site absolute value in any of the four bite conditions exhibited SED values above 4500 mJ. To detect any differences between the SED values between the different dietary niches we

conducted phylogenetic ANOVA tests at sample site 2, the area often exhibiting the highest levels of SED. These revealed no statistically significant differences between trophic groups in any loading condition. When scaled to be the equivalent volume of *Canis lupus* several of the smaller species had canine bite midline SE values above 10,000 mJ, with *Otocyon megalotis* exceeding 20,000 mJ and *Vulpes zerda* exceeding 30,000mJ. Again, to detect any differences between the scaled SED values between the different dietary niches we conducted Phylogenetic ANOVA tests at sample site 2. The scaled SED value results showed that there were differences between the dietary groups during carnassial occlusal (P -value 0.015) and carnassial wide biting (P -value 0.05). Pairwise post hoc tests revealed that in carnassial occlusal biting the generalists were significantly different from both the small prey specialists and the hypercarnivores where the scaled SED values of the generalists were greater than those of the other groups. For carnassial wide biting however, pairwise post hoc tests were unable to determine which pairs of groups were different. For illustration, raw and scaled values from sample site 2, are reported in Table 5 and illustrated in Fig. 8.

Colour maps were generated to allow for wider visual analysis of SED distribution in the skulls. The four loading conditions are shown in *Canis lupus*, for illustration (Fig.9), but similar patterns were recorded in all species. In all models the zygomatic arch experiences high SED, particularly along the ventral aspect. In canine biting, the caudal rostrum both dorsally (made up of the caudal parts of nasal and maxilla bones) and ventrally (made up of the caudal parts of the palatine and maxilla bones) also exhibits high SED. This is more marked at wide gape when the areas of high SED on the dorsal rostrum are contiguous with the areas of high SED on the ventral rostrum and zygomatic arches. The ventral orbital region made up of the zygomatic, lacrimal, maxilla and palatine bones, exhibits high SED at both canine and carnassial wide gape bites. SED in the cranial region of the skull alters from having a dorsal and rostral focus across the frontal bones at occlusal bite, to having a ventral and lateral focus on the parietal and temporal region at wide gape.

Mechanical advantage

Values for MA are shown in Table 6, and results from statistical analyses in the supplementary material. MA of the temporalis at canine bite was between 0.20 and 0.30. All of the hypercarnivore species were grouped at the top end of the range, the small prey specialists in the middle, and the generalists at the low end. Phylogenetic ANOVA results showed that there were differences between the dietary groups (P -value 0.0009), and the pairwise post hoc analysis revealed that the hypercarnivores were significantly different from both the generalists and the small prey specialists. MA of the masseter at canine bite was between 0.143 and 0.406. The hypercarnivores grouped together near the top end of the range and the small prey specialists grouped together near the bottom end of the range.

However, the generalists were split, with two species, *Otocyon megalotis* and *Nyctereutes procyonoides*, having the highest MA of the masseter at canine bite, and one species, *Vulpes zerda*, having the lowest. Phylogenetic ANOVA results showed that there were no statistically significant differences between the groups. MA of the temporalis at carnassial bite was between 0.344 and 0.596 with all of the hypercarnivore species at the top end of the range, the small prey specialists in the middle, and the generalists at the low end. Phylogenetic ANOVA results showed that there were statistically significant differences between the dietary groups (P -value 0.006), and the pairwise post hoc tests revealed that the generalists were significantly different from the hypercarnivores. MA of the masseter at carnassial bite was between 0.253 and 0.680 with all of the hypercarnivore species grouped toward the top end of the range, the small prey specialists grouped together near the bottom of the range. Again, the generalist group showed a wide range of MA, with *Otocyon megalotis* and *Nyctereutes procyonoides* having the highest values of all species, and *Vulpes corsac* one of the lowest. Phylogenetic ANOVA results showed that there were no statistically significant differences between the groups. The high MA values for the masseter exhibited by *Otocyon megalotis* and *Nyctereutes procyonoides* were due to the large in-lever values, which in turn were due to the large pre-angular processes.

Temporalis muscle angles relative to the occlusal plane

Results are reported in Table 7 and illustrated in Fig. 10. The superficial temporalis had a mean line of action of 142.6° relative to the occlusal plane, and there were no statistically significant differences between the dietary groups, phylogenetic ANOVA. The deep temporalis had a mean line of action of 119.9° relative to the occlusal plane. All hypercarnivore species values were below the mean and all generalist values were greater than the mean, indicating that the hypercarnivore species have more vertically aligned deep temporalis muscle fascicles, and the generalists have more horizontally aligned deep temporalis muscle fascicles. The phylogenetic ANOVA results showed significant differences between the groups (P -value 0.009) and the pairwise post hoc tests revealed that the hypercarnivore angles were significantly different to the generalists. The suprazygomatic temporalis had a mean line of action of 142.3° . All the generalist species values were above the mean and phylogenetic ANOVA results showed significant differences between the groups (P -value 0.009). The post hoc analysis reported that the generalists were significantly different to both the hypercarnivores and small prey specialists.

DISCUSSION

Canid jaw adductor muscles and their relationships to the bony morphology of the head were explored to reveal differences in masticatory function. Two hypotheses were

considered in relation to dietary niche. Before discussing the findings, it should be noted that the limited sample size, dictated by the laborious methodology and the scarcity of fresh material, does place certain restrictions on our analyses, albeit commensurate with previous studies (Hartstone-Rose *et al.*, 2012; Terhune *et al.*, 2015; Cox and Baverstock, 2016; Fabre *et al.*, 2017; Taylor *et al.*, 2018). Here we can only determine whether dietary extremes are similarly matched by distinct phenotypes as opposed to, for example, more nuanced shifts of form on a similar Canidae bauplan, perhaps coupled with behavioural adaptations. We contend that this broader evaluation and the accompanying insights into the transfer of muscle force into bite force represent a significant contribution to our understanding of these species and masticatory performance in general.

Hypothesis 1. There are significant relative, as well as absolute, differences of muscle force and bite force that reflect canid dietary niches.

This hypothesis was not strongly supported. Species tend to follow the same generalized size scaling trends, which appear to be predominantly isometric, though weak patterns of allometry may be hidden within the sample noise. A possible exception to isometry was temporalis muscle force vs occlusal bite forces. Regression confidence intervals indicate that as absolute temporalis muscle force increased, occlusal canine and carnassial bite forces increased at a greater rate. This suggests that although temporalis force production is relatively lower in larger species due to the muscle architecture, the geometry of the skull and mandible compensate for this, which results in isometric or positively scaling bite forces. As expected, muscle architecture has a clear influence on muscle force production and we found that individual muscle force contributions to overall muscle force do not reflect muscle mass contribution. The temporalis ‘underperforms’, that is, it contributes a mean 62% of mass but only a mean 52% of force production, whereas the masseter and pterygoid both ‘over perform’, i.e. they both contribute a greater percentage of force production than their percentage contribution toward the overall muscle mass. This disparity is attributable to the longer fascicle lengths of the larger temporalis affecting force production. In the RPCSA calculation, muscle mass is divided by fascicle length, and so RPCSA value is inversely proportional to the fascicle length. Muscles with absolutely longer fascicles are proportionally weaker than those with short fascicles.

Some previous FE studies (Slater *et al.* 2009; Tseng & Wang, 2010) have applied muscle forces to skulls in proportion to their mass which may lead to the incorrect weighting of muscle force application. The temporalis does, however, still contribute the greatest share of both muscle mass and force. Despite the relative force production inefficiency of the temporalis, the more caudal and dorsal siting of both its origin and insertion, when compared to those of the masseter, mean that it has a less limiting effect on the gape of the jaw, and consequently the longer fascicles are advantageous in species requiring a wide gape. The influence of taking the muscle architecture into account can also be seen when comparing

the interspecific muscle forces that were derived from the RPCSA method, to those we calculated using the dry skull method. As the dry skull method calculates cross-sectional area values only, it simply scales up force in direct proportion to area. As it does not consider the influence of the muscle architecture it cannot discriminate the functional differences between large and small muscles and also by extension, between large and small species. We found that within our dataset the dry skull method calculated higher muscle forces in large species, and lower muscle forces in small species, when compared to those calculated by the RPCSA method. This led to the dry skull method indicating that temporalis force scales with positive allometry in regression tests, whilst the RPCSA method indicates it scales with no marked allometric trend. Loading the FEA models with higher muscle input forces would result in higher output forces, i.e. increased bite forces. Absolutely higher temporalis forces for large species were predicted by Christiansen and Adolfssen (2005) using the dry skull method, than those predicted by us for the same species using the RPCSA method. They, and Damasceno *et al.* (2013), using the dry skull method, predicted higher bite forces in most of the larger species and predicted slightly lower bite forces in the smaller species. However, as the regression analyses between the two differently derived muscle force values showed no statistically significant differences between the two groups, although this may be due to the small sample size. The differences in absolute values are small, and dry skull derived values are a good approximation of RPCSA values where dissection derived data is unobtainable. Clearly, the level of muscle architectural detail required depends on the question and there seems little added value in employing more intricate and time-consuming approaches such as acid digestion when considering the broad functional differences addressed here. However, the additional specificity provided by such methods is likely to be important in, for example, intraspecific studies of dietary adaptation. A direct and controlled comparison of the fibre lengths measured using dissection only versus dissection and acid digestion is therefore warranted. As far the authors are aware no such study exists. Davis *et al.* (2010) have published an interesting comparison in bats of the dry skull method against PCSA calculated using acid digestion. They report that the dry skull method offers a reasonable approximation overall, overestimating masseter PCSA and under-estimating temporalis PCSA in comparison to acid digestion. Similar findings were observed in musteloid species when dissection derived data were compared with dry skull derived data, in that both methods gave comparable resultant bite force values (Hartstone-Rose *et al* 2019). Our findings for bite force concur that dry skull estimates of muscle force are reasonably well aligned to PCSA derived predictions. However, we found that temporalis force was slightly overestimated in large species and slightly underestimated in small species using the dry skull method. This is most likely due to the wide range of body masses seen in the canid dataset, where temporalis fascicle lengths, which are negatively correlated with PCSA values, were more than three times greater in the larger species than in the smaller species.

Hypothesis 2. The efficacy of muscle force production and its conversion into bite force, is indicative of different dietary niches.

There were demonstrable differences in efficiency between all four bite conditions. Carnassial bite at occlusion produced the highest bite force and is the most mechanically efficient. The greatest midline SED values were found at both closed and wide canine gape, revealing that canine biting is the most biomechanically testing and the least energetically efficient loading condition. Areas under greatest burden during canine biting were identified as the zygomatic arches and caudal rostrum, both dorsally and ventrally. It is difficult to know how functionally important this is, as all species can clearly accommodate the energy expenditure required, and phylogenetic ANOVA revealed no statistically significant differences between the SED values between the dietary groups. However, when small species were scaled to the size of the largest canid species, their skull shapes exhibited much higher values of SED than were seen in any unscaled models, demonstrating up to a fifty-fold increase in their original SED values, which may indicate that they would be structurally untenable if 'scaled up'. As SED is proportional to stress this may lead to ductile failure as well as being an energetic constraint. Generalists had higher values of SED than both the small specialists and hypercarnivores at all bite conditions, although phylogenetic ANOVA showed that these differences were only significant at the carnassial occlusal and possibly carnassial wide, bites. These findings may imply a limitation on the size of specific morphologies, which suggests some evidence of specialist function of shape (see Fig.6 Penrose *et al.* 2016). Earlier work (Penrose *et al.*, 2016) also highlighted a scaling component to head shape adaptation, where larger species exhibit cranial shape changes to accommodate isometrically scaling muscles on crania that must also house negatively scaling brain volumes. These findings suggest that the ability to withstand generated forces and the ability to house masticatory muscles are both factors in adaptive shape changes seen in canids.

Mechanical advantage calculations for the temporalis muscle, unlike the mechanical efficiency calculations, were able to distinguish between the dietary specialisms. This may be attributable to the MA methods more accurately describing the morphology of the different skulls rather than a simple force input/force output calculation. Calculations revealed that the temporalis had greater MA in the hypercarnivores than the other two trophic groups, indicating that the mandibular morphology of the jaw in these species is advantageous to force transmission. The increased MA may go some way to offsetting the disadvantage of longer temporalis fascicles in the large species. *Speothos venaticus*, the only small hypercarnivore, exhibits a mechanically advantageous skull shape combined with a small body mass and in turn has the greatest positive residuals in all body mass vs bite

1 force regressions. The masseter MA did not have any trophic group differentiation, although
2 the specific morphology of the two species with a pronounced subangular process (*Otocyon*
3 and *Nyctereutes*), had a very marked influence on MA for this muscle in these species.
4 Again, this did not result in any clear advantage of bite force, but it may be used to offset the
5 disadvantage of having an extra-long tooth row, in *Otocyon megalotis* at least. It was also
6 noticeable that although these two species had the highest MA values for the masseter, they
7 had amongst the lowest for the temporalis, so perhaps the masseter compensates and
8 contributes a higher proportion of muscle force toward bite force in these species. This
9 muscle arrangement may also align with the more pronounced grinding function associated
10 with the caudal teeth in these species. Possible future studies could consider running
11 models with muscles sequentially removed, following previous studies (Cox *et al.* 2013; Cox,
12 2017) to establish how individual muscles contribute to bite force outputs.

13
14 The line of action of temporalis revealed trophic group differentiation in two of the three
15 muscle subdivisions. As well as potentially increasing bite force this may also have other
16 functional outcomes. Sophisticated dynamic modelling, using multibody dynamic analyses
17 for example, has not yet been explored in canids, however previous work on bats (Reduker,
18 1983) and shrews (Fearnhead *et al.* 1955) has described how the angle of the line of action
19 of the temporalis influences bite force and speed of jaw closure. They concluded that
20 species with more vertically orientated temporalis lines of action are able to close their jaws
21 with greater force by pulling the coronoid process of the mandible dorsally, whilst species
22 with a more horizontal line of temporalis action are able to close their jaws more quickly by
23 pulling the coronoid process caudally. These contrasting dynamic strategies are reflected in
24 observed canid hunting behaviours: the pack hunting hypercarnivores kill by many sustained
25 bites, whereas species taking small prey utilise their fast closing jaws for relatively short
26 periods of time. Future work could consider histological analysis of muscle fascicles from the
27 three trophic groups to determine if their fibres contain a similar distribution of muscle fibre
28 types.

29
30 This work demonstrates that inclusion of muscle architectural details, however simplified,
31 has an effect of muscle force calculation, and that the siting of muscles on the skull may also
32 influence bite speed. The mechanical responses of the skull were assessed using analysis
33 of the FE models. In contrast to previous interspecific canid studies (Christiansen &
34 Adolfssen, 2005; Wroe *et al.* 2005; Christiansen & Wroe, 2007; Slater *et al.* 2009) we
35 created our models using empirically derived specimen-specific muscle forces. The
36 improved accuracy of the loading conditions allowed us to use a modelling method that
37 takes into account both size and shape differences between species. The FE models
38 indicated the highest SED at canine biting, particularly in the caudal rostrum. Given that
39 canine biting appears to be the least efficient and most biomechanically demanding

condition, it may represent the limiting factor on skull performance. As canine biting chiefly occurs during the capture, restraint and killing of prey, it is fundamental to predatory success, and limitations on canine bite performance must be an important factor in determining trophic niche.

We established that bite forces do not scale with a marked allometric trend, but that individual species have morphological compensatory techniques to achieve similar relative outputs. The link between mechanical performance and whole organism performance is poorly understood (Dumont *et al.* 2011) and by considering only two functional elements of bite performance, the skull and masticatory muscles, other potentially important factors were overlooked. These include the role of the neck muscles, the effect of supporting the mass of the skull and mandible, anchorage of the tooth roots in the alveoli, and the uniting role of other soft tissue structures. Soft-tissue structures, such as tendon, connective tissue and muscle fascia may facilitate integration of separate elements during biting. During our dissection work we noted that the muscle fascia covering temporalis was particularly thick, and was contiguous with the fascia and periosteum covering the zygomatic arch, and then ran down onto the masseter muscle, in effect unifying all of these functional units. We also noted that some temporalis and masseter muscle fascicles appeared to arise from their covering fascia, although this would need to be confirmed using histological techniques. Curtis *et al.* (2011) have explored the role of the fascia in macaques during biting, and concluded, using FE analysis, that the temporal fascia has an impact on biomechanical function by opposing the pull of the masseter on the zygomatic arches, greatly reducing localized strains. If future FE work on canids could include data on these poorly reported structures, this may further improve the accuracy of modelling techniques.

CONCLUSION

Canids may be constrained in adaptability and have remained as functional generalists, never exploring the highly specialized niches that, for instance, the felids have exploited. Divergence of canids into hypercarnivory may rely more on behavioral rather than functional adaptations, as the ability to tackle large prey relies on working in packs, rather than changing morphology to increase relative bite force. The inclusion of muscle architectural detail is shown to influence masticatory muscle force production capability calculations, indicating that muscles with longer fascicles were disadvantaged compared to muscles with shorter fascicles. However, compensatory morphological features allow bite forces to scale isometrically or with weak positive allometry. Dietary groups were differentiated by temporalis fascicle angles, which, when allied with the differentiation of rostral length reported in previous studies (Van Valkenburgh & Koepfli, 1993; Slater *et al.* 2009; Penrose *et al.* 2016) may further contribute to specialisations of fast jaw closing or forceful jaw closing species. The most biomechanically demanding masticatory function is canine biting, and the

highest strain energy values were reported in this condition, particularly in the zygomatic arches and caudal rostrum. Specific head shapes may be constrained by size, with scaled strain energy models predicting that some bony morphologies may only be viable in species with small body masses.

This study is the most comprehensive investigation of the biomechanics of canid biting to date. It provides important insights into morphological versus behavioral adaptive strategies to different dietary niches and will inform future comparative studies, in particular the building of computational models and estimations of bite force production.

Acknowledgements:

We would like to thank our editor Professor Tim Smith and two anonymous reviewers for their comments and suggestions. We would also like to thank Dr Andrew Kitchener and Georg Hantke at the National Museums of Scotland, Katie McDonald at the West Midland Safari Park, Zak Showell at Twycross Zoo, Julia Coats at the Animal and Plant Health Agency (APHA) and staff at Chester Zoo for the donation of specimens. We would also like to thank Fraser McConnell and Martin Baker at the University of Liverpool for CT scanning, and staff at Liverpool Magnetic Resonance Imaging Centre (LiMRIC) for MR scanning. The authors have no conflict of interest to declare.

Author contributions:

Data collection, imaging, dissection, analysis and manuscript development was conducted by FP. PC performed the phylogenetic comparative methods. NJ and PC aided in concept development, and NJ, PC and GK all aided in critical revision of the manuscript.

Literature Cited

- Anapol FC, Barry K** (1996) Fiber architecture of the extensors of the hindlimb in semiterrestrial and arboreal guenons. *Am J Phys Anthropol* **99**, 429–447.
- Andersson K** (2005) Were there pack-hunting canids in the Tertiary, and how can we know? *Paleobiol* **31**, 56–72.
- Attard MRG, Chamoli U, Ferrara TL, Rogers TL, Wroe S** (2011) Skull mechanics and implications for feeding behaviour in a large marsupial carnivore guild: The thylacine, Tasmanian devil and spotted-tailed quoll. *J Zool* **285**, 292–300.
- Auperrin A, Delille R, Lesueur D, Bruyere K, Masson C, Drazetic P** (2014) Geometrical and material parameters to assess the macroscopic mechanical behaviour of fresh cranial bone samples. *J Biomech* **47**, 1180–1185.
- Boruah S, Subit D, Paskoff G, Shender B, Crandall J, Salzar R** (2017) Influence of bone microstructure on the mechanical properties of skull cortical bone – a combined experimental and computational approach. *J Mech Behavior Biomed Mater* **65**, 688–704.
- Bright JA, Rayfield EJ** (2011) The response of cranial biomechanical finite element models to variations in mesh density. *Anat Rec* **294**, 610–620.
- Burgin CJ, Colella JP, Kahn PL, Upham NS** (2018) How many species of mammal are there? *J Mammal* **99**, 1-14.
- Butler DL, Guan Y, Kay M, Cummings JF, Feder SM, Levy MS** (1992) Location-dependent variations in the material properties of the anterior cruciate ligament. *J Biomech* **25**, 511–518.
- Cheung JT-M, Zhang M, Leung AK-M, Fan Y-B** (2005) Three-dimensional finite element analysis of the foot during standing - a material sensitivity study. *J Biomech* **38**, 1045–1054.
- Christiansen P, Adolfssen JS** (2005) Bite forces, canine strength and skull allometry in carnivores (Mammalia, Carnivora). *J Zool* **266**, 133–151.
- Christiansen P and Wroe S** (2007) Bite forces and evolutionary adaptations to feeding ecology in carnivores. *Ecology* **88**, 347–358.
- Colombo V, Cadova M, Gallo LM** (2013) Mechanical behavior of bovine nasal cartilage under static and dynamic loading, *J Biomech* **46**, 2137 - 2144.
- Correro-Shahgaldian MR, Introvigne J, Ghayor C, Weber FE, Gallo LM, Colombo V** (2016) Properties and mechanobiological behavior of bovine nasal septum cartilage. *Ann Biomed Eng* **44**, 1821–1831.
- Cox PG, Rayfield EJ, Fagan MJ, Herrel A, Pataky TC, Jeffery N** (2012) Functional evolution of the feeding system in rodents. *PLoS ONE* **7**, e36299.
- Cox PG** (2017) The jaw is a second-class lever in *Pedetes capensis* (Rodentia : Pedetidae). *PeerJ* **5**, e3741
- Cox PG, Kirkham J, Herrel A** (2013) Masticatory biomechanics of the Laotian rock rat, *Laonastes aenigmamus*, and the function of the zygomaticomandibularis muscle. *PeerJ* **1**, e160.
- Cox PG, and Baverstock H** (2016) Masticatory Muscle Anatomy and Feeding Efficiency of the American Beaver, *Castor canadensis* (Rodentia, Castoridae). *Journal of Mammalian*

- Evolution*. Journal of Mammalian Evolution, 23(2), pp. 191–200.
- Curtis N, Witzel U, Fitton L, O'Higgins P, Fagan M** (2011) The mechanical significance of the temporal fasciae in macaca fascicularis: an investigation using finite element analysis. *Anat Rec* **294**, 1178–1190.
- Damasceno EM, Hingst-Zaher E, Astua D** (2013) Bite force and encephalization in the Canidae (Mammalia: Carnivora). *J Zool* **290**, 246–254.
- Davis JL, Santana SE, Dumont ER and Grosse IR** (2010) Predicting bite force in mammals : two-dimensional versus three-dimensional lever, (1), pp. 1844–1851.
- Douglass JK, Wcislo WT** (2010) An inexpensive and portable microvolumeter for rapid evaluation of biological samples. *Biotechniques* **49**, 566–572.
- Dumont ER, Davis JL, Grosse IR, Burrows AM** (2011) Finite element analysis of performance in the skulls of marmosets and tamarins. *J Anat* **218**, 151–162.
- Dumont ER, Grosse IR, Slater GJ** (2009) Requirements for comparing the performance of finite element models of biological structures. *J Theor Biol* **256**, 96–103.
- Evans HE, De Lahunta A** (2013) *Miller's Anatomy of the Dog*. 4th ed. Philadelphia:Saunders
- Fabre PH, Herrel A, Fitriana Y, Meslin L and Hautier L** (2017) Masticatory muscle architecture in a water-rat from Australasia (Murinae, Hydromys) and its implication for the evolution of carnivory in rodents. *Journal of Anatomy*, (June), pp. 380–397.
- Falland-Cheung L, Waddell JN, Li KC, Tong D, Brunton P** (2017) Investigation of the elastic modulus, tensile and flexural strength of five skull simulant materials for impact testing of a forensic skin/skull/brain model. *J Mech Behavior Biomed Mater* **68**, 303–307.
- Fearnhead RW, Shute CCD, Bellairs AD** (1955) The temporo-mandibular joint of shrews. *Proc Zool Soc Lond* **125**, 795–806.
- Figueirido B, Macleod N, Krieger J, De Renzi M, Perez-Claros JA, Palmqvist P** (2011) Constraint and adaptation in the evolution of carnivoran skull shape. *Paleobiol* **37**, 490–518.
- Forbes-Harper JL, Crawford HM, Dundas SJ et al.** (2017) Diet and bite force in red foxes: ontogenetic and sex differences in an invasive carnivore. *J Zool* **303**, 54–63.
- Freckleton RP** (2009) The seven deadly sins of comparative analysis. *J Evol Biol* **22**, 1367–1375.
- Freckleton RP, Harvey PH, Pagel M** (2002) Phylogenetic analysis and comparative data: a test and review of evidence. *Am Nat* **160**, 712–726.
- Gans C** (1982) Fiber architecture and muscle function. *Exerc Sport Sci Rev* **10**, 160–207.
- Garland T, Dickerman AW, Janis CM, Jones JA** (1993) Phylogenetic analysis of covariance by computer simulation. *Syst Biol* **42**, 265–292.
- Gittleman J L, Van Valkenburgh B** (1997) Sexual dimorphism in the canines and skulls of carnivores: effects of size, phylogeny, and behavioural ecology. *J Zool* **242**, 97–117.
- Goswami A, Milne N, Wroe S** (2011) Biting through constraints: cranial morphology, disparity and convergence across living and fossil carnivorous mammals. *Proc Roy Soc*

Lond **278**, 1831–1839.

Grellmann W, Berghaus A, Haberland E-J et al. (2006) Determination of strength and deformation behavior of human cartilage for the definition of significant parameters. *J Biomed Mater Res A* **78A**, 168–174.

Griffin MF, Premakumar Y, Seifalian AM, Szarko M, Butler PEM (2016) Biomechanical characterisation of the human nasal cartilages; implications for tissue engineering. *J Mater Sci: Mater Med* **27**, 11.

Habelitz S, Marshall SJ, Marshall GW, Balooch M (2001) Mechanical properties of human dental enamel on the nanometre scale. *Arc Oral Biol* **46**, 173–183.

Hammer Ø, Harper DAT, Ryan PD (2001) PAST: paleontological statistics software package for education and data analysis. *Palaeontol Elec* **4**, 9.

Harmon LJ, Weir JT, Brock CD, Glor RE, Challenger W (2008) GEIGER: investigating evolutionary radiations. *Bioinformatics* **24**, 129–131.

Hartstone-Rose A, Hertzog I, Dickinson E (2019) Bite force and masticatory muscle architecture adaptations in the dietarily diverse musteloidea (Carnivora). *Anat Rec* **302**, 2287–2299.

Hartstone-Rose A, Perry JMG, Morrow CJ (2012) Bite Force Estimation and the Fiber Architecture of Felid Masticatory Muscles. *Anat Rec* **295**, 1336–1351.

Haxton H (1944) Absolute muscle force in the ankle flexors of man. *J Physiol* **103**, 267–273.

He LH, Fujisawa N, Swain MV (2006) Elastic modulus and stress-strain response of human enamel by nano-indentation. *J Biomat* **27**, 4388–4398.

Herring SW (2007) Masticatory muscles and the skull: a comparative perspective. *Archives of Oral Biology*, **52**, 296–299.

Herring SW, Rafferty KL, Liu ZJ, Lemme M (2011) Mastication and the postorbital ligament: Dynamic strain in soft tissues. *Integr Comp Biol* **51**, 297–306.

Huq E, Wall CE, Taylor AB (2015) Epaxial muscle fiber architecture favors enhanced excursion and power in the leaper *Galago senegalensis*. *J Anat* **227**, 524–540.

Jensen RH, Davy DT (1975) An investigation of muscle lines of action about the hip: A centroid line approach vs the straight line approach. *J Biomech* **8**, 105–110.

Kawamura Y, Kato I, Miyoshi K (1968) Functional Anatomy of the Lateral Pterygoid Muscle in the Cat. *Journal of Dental Research*, **47**, 1142–1148.

Kembel SW, Cowan PD, Helmus MR, Cornwell WK, Morlon H, Ackerly DD, Blomberg SP, Webb CO (2010) Picante: R tools for integrating phylogenies and ecology. *Bioinformatics* **26**, 1463–1464.

Kim S-I, Suzuki S, Oh J et al. (2012) Sexual dimorphism of craniodental morphology in the raccoon dog *Nyctereutes procyonoides* from South Korea. *J Vet Med Sci* **74**, 1609–1616.

Kinney J H, Marshall SJ, Marshall GW (2003) The mechanical properties of human dentin: a critical review and re-evaluation of the dental literature. *Crit Rev Oral Biol Med* **14**, 13–29.

Koolstra JH, van Eijden TMGJ, Weijs WA, Naeije M (1988) A three-dimensional mathematical model of the human masticatory system predicting maximum possible bite

forces. *J Biomech* **21**, 563–576.

Kumaresan S, Yoganandan N, Pintar F, Voo LM, Cusick JF, Larson SJ (1997) Finite element modeling of cervical laminectomy with graded facetectomy. *J Spinal Disorders* **10**, 40–46.

Kupczik K, Dobson CA, Fagan MJ, Crompton RH, Oxnard CE, O'Higgins P (2007) Assessing mechanical function of the zygomatic region in macaques: validation and sensitivity testing of finite element models. *J Anat* **210**, 41–53.

Leary RP, Manuel CT, Shamouelian D et al. (2015) Finite element model analysis of cephalic trim on nasal tip stability. *JAMA Fac Plast Surg* **17**, 413–420.

Lindblad-Toh K, Wade CM, Mikkelsen TS, Karlsson EK, Jaffe DB, Kamal M, Clamp M, Chang JL, Kulbokas III EJ, Zody MC, Mauceli E (2005) Genome sequence, comparative analysis and haplotype structure of the domestic dog. *Nature* **438**, 803–819.

Maas SA, Ellis B, Ateshian G, Weiss J (2012) FEBio: Finite Elements for Biomechanics. *J Biomech Eng* **134**, 011005.

Macdonald D (2009) *The Encyclopedia of Mammals*. Oxford: Oxford University Press.

Macdonald DW, Sillero-Zubiri C (2004) *The Biology and Conservation of Wild Canids*. Oxford: Oxford University Press.

Margulies SS, Thibault KL (2000) Infant skull and suture properties: measurements and implications for mechanisms of pediatric brain injury. *J Biomech Eng* **122**, 364–371.

McHenry CR, Clausen PD, Daniel WJT, Meers MB, Pendharkar A (2006) Biomechanics of the rostrum in crocodilians: a comparative analysis using finite element modelling. *Anat Rec* **288A**, 827–849.

Meloro C, Hudson A, Rook L (2015) Feeding habits of extant and fossil canids as determined by their skull geometry. *J Zool* **295**, 178–188.

Mohamed ANA, Brown, MA, Shabana AA (2010) Study of the ligament tension and cross-section deformation using nonlinear finite element/multibody system algorithms. *Multibody Syst Dynam* **23**, 227–248.

Motherway JA, Verschueren P, Van der Perre G, Sloten JV, Gilchrist MD (2009) The mechanical properties of cranial bone: The effect of loading rate and cranial sampling position. *J Biomech* **42**, 2129–2135.

Murphy RA, Beardsley AC (1974) Mechanical properties of the cat soleus muscle in situ. *Am J Physiol* **227**, 1008–1013.

Nowak R (2005) *Walker's Carnivores of the World*. Baltimore: Johns Hopkins University Press

Nyakatura K, Bininda-Emonds OR (2012) Updating the evolutionary history of Carnivora (Mammalia): a new species-level supertree complete with divergence time estimates. *BMC biology* **10**, 12.

Orme CDL (2012) *The caper package: comparative analyses in phylogenetics and evolution in R*. <http://caper.r-forge.r-project.org>

Paradis E, Claude J, Strimmer K (2004) APE: analyses of phylogenetics and evolution in R language. *Bioinformatics* **20**, 289–290.

- Pennell MW, Eastman JM, Slater GJ, Brown JW, Uyeda JC, Fitzjohn RG, Alfaro ME, Harmon LJ** (2014) geiger v2.0: an expanded suite of methods for fitting macroevolutionary models to phylogenetic trees. *Bioinformatics* **15**, 2216-2218.
- Penrose F, Kemp GJ, Jeffery N** (2016) Scaling and accommodation of jaw adductor muscles in Canidae. *Anat Rec* **299**, 951–966.
- Peterson J, Dechow PC** (2002) Material properties of the inner and outer cortical tables of the human parietal bone. *Anat Rec* **268**, 7–15.
- Pinheiro J, Bates D, Debroy S, Sarkar D, R Core Team** (2016) *nlme: Linear and Nonlinear Mixed Effects Models* (R package version 3.1-111).
- Preuschoft H, Witzel U** (2005) Functional shape of the skull in vertebrates: which forces determine skull morphology in lower primates and ancestral synapsids? *Anat Rec* **283A**, 402–413.
- Prevosti FJ, Turazzini GF, Ercoli MD, Hingst-Zaher E** (2012) Mandible shape in marsupial and placental carnivorous mammals: a morphological comparative study using geometric morphometrics. *Zool J Linn Soc* **164**, 836–855.
- Radhakrishnan P, Mao JJ** (2004) Nanomechanical properties of facial sutures and sutural mineralization front. *J Dent Res* **83**, 470–475.
- Radinsky LB** (1981) Evolution of skull shape in carnivores. I. Representative modern carnivores. *Biol J Linn Soc* **15**, 369–388.
- Rayfield EJ, Norman DB, Horner CC, et al.** (2001) Cranial design and function in a large theropod dinosaur. *Nature* **409**, 1033– 1037.
- Reduker DW** (1983) Functional analysis of the masticatory apparatus in two species of *Myotis*. *J Mammal* **64**, 277–286.
- Revell LJ** (2012) phytools: An R package for phylogenetic comparative biology (and other things). *Methods Ecol Evol* **3**, 217–223.
- Rho JY, Ashman RB, Turner CH** (1993) Young's modulus of trabecular and cortical bone material: ultrasonic and microtensile measurements. *Journal of biomechanics*, **26**, 111-119.
- Rho JY, Tsui TY, Pharr GM** (1997) Elastic properties of human cortical and trabecular lamellar bone measured by nanoindentation. *Biomaterials* **18**, 1325–1330.
- Ryan SD, Williams JL** (1989) Tensile testing of rodlike trabeculae excised from bovine femoral bone. *J Biomech* **22**, 351–355.
- Sacco T, Van Valkenburgh B** (2004) Ecomorphological indicators of feeding behaviour in the bears (Carnivora: Ursidae). *J Zool* **263**, 41–54.
- Schneider C, Rasband WS, Eliceiri KW** (2012) NIH Image to ImageJ: 25 years of image analysis. *Nat Methods* **9**, 671–675.
- Segura V, Prevosti F** (2012) A quantitative approach to the cranial ontogeny of *Lycalopex culpaeus* (Carnivora: Canidae). *Zoomorphol* **131**, 79–92.
- Senawongse P, Otsuki M, Tagami J, Mjör I** (2006) Age-related changes in hardness and modulus of elasticity of dentine. *Archives of Oral Biology*, **51**, 457-463.

- Sillero-Zubiri C, Hoffmann M, Macdonald DW** (2004) *Canids: Foxes, Wolves, Jackals and Dogs: status survey and conservation action plan*. Gland, Switzerland: IUCN.
- Singh B, Klimek J, Dyce KM, Sack WO, Wensing C JG** (2018) *Dyce, Sack, and Wensing's textbook of veterinary anatomy*. 5th ed. St. Louis, Missouri : Elsevier
- Slater G J, Dumont ER, Van Valkenburgh B** (2009) Implications of predatory specialization for cranial form and function in canids. *J Zool* **278**, 181–188.
- Ström D, Holm S, Clemensson E, Haraldson T, Carlsson GE** (1988) Gross anatomy of the craniomandibular joint and masticatory muscles of the dog. *Archives of Oral Biology*, **33**, 597–604.
- Tanner JB, Zelditch ML, Lundrigan BL, Holekamp KE** (2010) Ontogenetic change in skull morphology and mechanical advantage in the spotted hyena (*Crocuta crocuta*). *J Morphol* **271**, 353–365.
- Taylor AB, Terhune CE, Toler M, Holmes M, Ross CF and Vinyard CJ** (2018) Jaw-Muscle Fiber Architecture and Leverage in the Hard-Object Feeding Sooty Mangabey are not Structured to Facilitate Relatively Large Bite Forces Compared to Other Papionins. *Anatomical Record*, 342(August 2017), pp. 325–342.
- Taylor AB, Vinyard CJ** (2013) The relationships among jaw-muscle fiber architecture, jaw morphology, and feeding behavior in extant apes and modern humans. *Am J Phys Anthropol* **151**, 120–134.
- Terhune, CE, Hylander WL, Vinyard CJ, Taylor AB** (2015) Jaw-muscle architecture and mandibular morphology influence relative maximum jaw gapes in the sexually dimorphic *Macaca fascicularis*. *J Human Evol* **82**, 145–158.
- Thomason JJ** (1991) Cranial strength in relation to estimated biting forces in some mammals. *Can J Zool* **69**, 2326–2333.
- Thrall DE, Robertson ID** (2015) *Atlas of Normal Radiographic Anatomy and Anatomic Variants in the Dog and Cat*. 2nd ed. Philadelphia: Saunders.
- Tomo S, Nakajima K, Tomo I, Nodai E, Kobayashi, S** (1995) The morphology and innervation of the lateral pterygoid muscle of the dog. *Journal of Anatomy*, **186**, 435–9.
- Tseng ZJ, Wang X** (2010) Cranial functional morphology of fossil dogs and adaptation for durophagy in *Borophagus* and *Epiacyn* (Carnivora, Mammalia). *J Morphol* **271**, 1386–1398.
- Turnbull WD** (1970) Mammalian masticatory apparatus. *Fieldiana Geology*, **18**, 147–356.
- van Rietbergen B, Weinans H, Huiskes R, Odgaard A** (1995) A new method to determine trabecular bone elastic properties and loading using micromechanical finite-element models. *J Biomech* **28**, 69–81.
- Van Valkenburgh B** (1996) Feeding behavior in free-ranging, large African carnivores. *J Mammal* **77**, 240–254.
- Van Valkenburgh B, Koepfli K-P** (1993) Cranial and dental adaptations to predation in canids. *Symp Zool Soc Lond* **65**, 15–37.
- Vickerton P, Jarvis J, Jeffery N** (2013) Concentration-dependent specimen shrinkage in iodine-enhanced microCT. *J Anat* **223**, 185–193.

- 1 **Wainwright PC, Richard BA** (1995) Predicting patterns of prey use from morphology of
2 fishes. *Env Biol Fishes*, **44**, 97–113.
- 3
- 4 **Wang X, Tedford RH** (2010) *Dogs: Their Fossil Relatives and Evolutionary History*. New
5 York: Columbia University Press.
- 6
- 7 **Weed D, Maqueda LG** (2010) A new nonlinear multibody/finite element formulation for knee
8 joint ligaments. *Nonlinear Dynam* **60**, 357–367.
- 9
- 10 **Weijs WA, Hillen B** (1985) Cross-sectional area and estimated intrinsic strength of the
11 human jaw muscles. *Acta Morph Neerl-Scand* **23**, 267–274.
- 12
- 13 **Wozencraft W** (1993) Order Carnivora. In: *Mammal species of the world: a taxonomic and*
14 *geographic reference* (eds Wilson DE, Reeder DM), pp. 279-348. Washington DC:
15 Smithsonian Institution Press.
- 16
- 17 **Wroe S, McHenry C, Thomason J** (2005) Bite club: comparative bite force in big biting
18 mammals and the prediction of predatory behaviour in fossil taxa. *Proc R Soc B* **272**, 619–
19 625.
- 20
- 21 **Wroe S and Milne N**, (2007) Convergence and remarkably consistent constraint in the
22 evolution of carnivore skull shape. *Evolution* 61(5), pp.1251-1260.
- 23
- 24 **Zysset PK, Guo XE, Hoffer CE, Moore KE, Goldstein SA** (1999) Elastic modulus and
25 hardness of cortical and trabecular bone lamellae measured by nanoindentation in the human
26 femur. *J Biomech* **32**, 1005–1012.

	Sex	Phylogenetic group	Dietary specialization	Mean body mass (g) from literature ^{1,2}	Temporalis mass (g)	Mean temporalis fascicle Length (cm)	Masseter mass (g)	Mean masseter fascicle length (cm)	Pterygoid mass (g)	Mean pterygoid fascicle length (cm)	Total jaw adductor mass (g)	Temporalis force (N) from RPCSA	Masseter force (N) from RPCSA	Pterygoid force from RPCSA (N)	Temporalis force (N) from dry skull	Masseter force (N) from dry skull
<i>Alopex lagopus</i>	M	Fox-like	Small prey specialist	5200	43.8	2.4	14.9	1.5	4.47	1.9	63.1	530	251	82	336	298
<i>Canis lupus</i>	2M,1F	Wolf-like	Hypercarnivore	36500	179.5	4.3	84.5	2.7	25.7	2.5	289.7	1328	935	441	1432	823
<i>Canis mesomelas</i>	M	Wolf-like	Small prey specialist	9700	46.6	2.6	20.2	2.0	6.7	1.8	73.5	603	361	130	403	358
<i>Chrysocyon brachyurus</i>	F	South American	Small prey specialist	25000	106.1	4.5	61.5	2.7	13.2	2.1	180.8	852	770	220	900	775
<i>Cuon alpinus</i>	F	Wolf-like	Hypercarnivore	13500	81.6	4.2	40.6	2.8	10.4	2.4	132.6	753	508	151	777	523
<i>Lycaon pictus</i>	2M, 1F	Wolf-like	Hypercarnivore	26500	141.7	5.1	84.4	3.0	19.4	2.6	245.5	880	836	225	950	680
<i>Nyctereutes procyonoides</i>	M	Fox-like	Generalist	6500	19.9	1.8	10.6	1.4	3.2	1.2	33.7	360	262	95	341	212
<i>Otocyon megalotis</i>	M	Fox-like	Generalist	4200	13.5	1.9	6.6	1.0	2.2	0.8	22.4	252	227	99	231	212
<i>Speothos venaticus</i>	F	South American	Hypercarnivore	6500	42.7	2.7	24.6	1.9	5.1	1.9	72.4	559	442	94	370	289
<i>Vulpes corsac</i>	3M, 1F	Fox-like	Small prey specialist	2850	14.7	2.0	6.4	1.4	2.3	1.3	23.4	309	171	61	205	194
<i>Vulpes vulpes</i>	3M	Fox-like	Small prey specialist	8500	48	3.0	19.3	2.4	5.7	2.0	73	487	262	101	438	318
<i>Vulpes zerda</i>	F	Fox-like	Generalist	1150	5.6	1.4	2.4	0.8	0.9	1.2	8.9	127	96	26	97	85

Table 1. Details of specimens used in this study including body mass, jaw adductor muscle masses and forces as calculated by the RPCSA and dry skull methods.

	Previous studies		This study	
Material	Authors	Young's modulus	Young's modulus	Type
Cortical bone	Peterson & Dechow 2002; Motherway <i>et al.</i> 2009; Auperrin <i>et al.</i> 2014; Boruah <i>et al.</i> 2017;	3.81GPa - 21GPa	7 GPa	Isotropic elastic
Cancellous bone	Ryan & Williams, 1989; Rho <i>et al</i> 1993; van Rietbergen <i>et al.</i> 1995; Rho <i>et al.</i> 1997; Zysset <i>et al.</i> 1999	1GPa-14.8GPa	6Pa	Isotropic elastic
Teeth	Rayfield <i>et al.</i> 2001; Habelitz <i>et al</i> 2001 Kinney <i>et al.</i> 2003; He <i>et al</i> 2006; Senawongse <i>et al</i> 2006; Attard <i>et al.</i> 2011	14.5 - 100GPa	30Gpa	Isotropic elastic
Septum	Grellmann <i>et al.</i> 2006; Colombo <i>et al</i> 2013 Leary <i>et al.</i> 2015; Correro-Shahgaldian <i>et al.</i> 2016 Griffin <i>et al</i> 2016	0.5 - 168Mpa	9Mpa	Isotropic elastic
Zygomatic suture	Margulies & Thibault, 2000; Radhakrishnan & Mao, 2004; Kupczik <i>et al.</i> 2007	1.16MPa - 7.7Gpa	354MPa	Neohookian
Orbital ligament	Butler <i>et al.</i> 1992; Kumaresan <i>et al.</i> 1997; Cheung <i>et al.</i> 2005 Mohamed <i>et al.</i> 2010,	1.5- 284 MPa	100 MPa	Isotropic elastic

Table 2. Summary of material properties

Species	Muscle	Mass (g)	Predicted volume (cm ³)	Volume from microvolumeter
<i>Vulpes vulpes</i>	Suprazygomatic temporalis	2.84	2.69	2.60
	Superficial temporalis	21.80	20.64	20.10
	Deep temporalis	23.06	21.84	22.00
	Superficial masseter	9.40	8.90	9.00
	Deep masseter	5.32	5.04	4.70
	zygomaticomandibularis	4.56	4.32	4.30
	pterygoids	5.75	5.45	5.30
<i>Vulpes zerda</i>	Suprazygomatic temporalis	0.22	0.21	0.20
	Superficial temporalis	2.81	2.66	2.50
	Deep temporalis	2.57	2.43	2.40
	Superficial masseter	1.28	1.21	1.20
	Deep masseter	0.73	0.69	0.70
	zygomaticomandibularis	0.39	0.37	0.40
	pterygoids	0.90	0.85	0.84

Table 3. Jaw adductor muscle masses, predicted volumes and volumes from two species.

Species	Canine bite				Carnassial bite			
	Occlusion		Wide gape		Occlusion		Wide gape	
	BF (N)	ME	BF (N)	ME	BF (N)	ME	BF (N)	ME
<i>Alopex lagopus</i>	158	0.18	124	0.14	261	0.30	201	0.23
<i>Canis lupus</i>	508	0.19	295	0.11	715	0.26	495	0.18
<i>Canis mesomelas</i>	234	0.21	165	0.15	319	0.29	234	0.21
<i>Chrysocyon brachyurus</i>	246	0.13	225	0.12	384	0.21	355	0.19
<i>Cuon alpinus</i>	297	0.22	220	0.16	434	0.31	342	0.25
<i>Lycaon pictus</i>	384	0.20	223	0.11	534	0.27	345	0.18
<i>Nyctereutes procyonoides</i>	131	0.19	63	0.09	186	0.26	99	0.14
<i>Otocyon megalotis</i>	124	0.21	82	0.14	159	0.28	108	0.19
<i>Speothos venaticus</i>	222	0.20	192	0.18	319	0.29	301	0.28
<i>Vulpes corsac</i>	76	0.14	54	0.10	123	0.23	93	0.17
<i>Vulpes vulpes</i>	160	0.19	107	0.13	248	0.29	172	0.20
<i>Vulpes zerda</i>	27	0.11	24	0.10	45	0.18	44	0.18

Table 4. Bite force and mechanical efficiency.

Species	Sample site 2															
	Canine occlusion mJ				Canine wide mJ				Carnassial occlusion mJ				Carnassial wide mJ			
	original	Scaled to <i>C. lupus</i>	<i>C. lupus</i>	% of <i>C. lupus</i> SED	original	Scaled to <i>C. lupus</i>	<i>C. lupus</i>	% of <i>C. lupus</i> SED	original	Scaled to <i>C. lupus</i>	<i>C. lupus</i>	% of <i>C. lupus</i> SED	original	Scaled to <i>C. lupus</i>	<i>C. lupus</i>	% of <i>C. lupus</i> SED
<i>Alopex lagopus</i>	704	4448	2763	161	656	4145	3108	133	23	145	92	158	18	114	282	40
<i>Canis mesomelas</i>	4391	18414	2763	666	2976	12480	3108	402	158	663	92	720	137	575	282	204
<i>Chrysocyon brachyurus</i>	1323	2693	2763	97	2141	4357	3108	140	104	212	92	230	338	790	282	280
<i>Cuon alpinus</i>	1129	3467	2763	125	1340	4115	3108	132	114	350	92	380	47	144	282	51
<i>Lycaon pictus</i>	1130	1887	2763	68	1396	2331	3108	75	73	122	92	132	279	466	282	165
<i>Nyctereutes procyonoides</i>	907	7407	2763	268	727	5937	3108	191	81	661	92	719	86	702	282	249
<i>Otocyon megalotis</i>	1647	18645	2763	675	1894	21442	3108	690	128	1449	92	1575	313	3543	282	1257
<i>Speothos venaticus</i>	545	2326	2763	84	808	3449	3108	111	12	51	92	56	20	85	282	30
<i>Vulpes corsac</i>	778	10192	2763	369	780	10218	3108	329	20	262	92	285	99	1297	282	460
<i>Vulpes vulpes</i>	1299	8602	2763	311	1226	8118	3108	261	17	113	92	122	75	497	282	176
<i>Vulpes zerda</i>	464	23559	2763	853	637	32343	3108	1041	36	1828	92	1987	86	4367	282	1548

Table 5. Average node values from sample site two, at all four loading conditions. Absolute values and values when volume scaled to that of *C. lupus*.

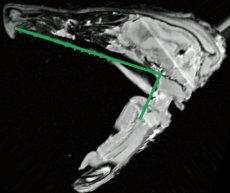
DIETARY GROUP	SPECIES	MA temporalis canine bite	MA masseter canine bite	MA temporalis carnassial bite	MA masseter carnassial bite
HYPERCARNIVORE	<i>Canis lupus signtaus</i>	0.26	0.22	0.52	0.45
	<i>Cuon alpinus</i>	0.28	0.21	0.55	0.40
	<i>Lycaon pictus</i>	0.26	0.23	0.50	0.44
	<i>Speothos venaticus</i>	0.30	0.24	0.60	0.47
SMALL PREY SPECIALIST	<i>Alopex lagopus</i>	0.24	0.15	0.39	0.25
	<i>Canis mesomelas</i>	0.24	0.19	0.46	0.37
	<i>Chrysocyon brachyurus</i>	0.21	0.18	0.41	0.35
	<i>Vulpes corsac</i>	0.23	0.15	0.49	0.31
	<i>Vulpes vulpes</i>	0.25	0.16	0.49	0.31
GENERALIST	<i>Nyctereutes procyonoides</i>	0.21	0.41	0.36	0.68
	<i>Otocyon megalotis</i>	0.20	0.37	0.34	0.62
	<i>Vulpes zerda</i>	0.20	0.14	0.41	0.29

Table 6. Mechanical advantage

	Superficial temporalis	Deep temporalis	Suprazygomatic temporalis
<i>Alopex lagopus</i>	145.69	120.90	138.90
<i>Canis lupus signtaus</i>	141.50	109.50	138.49
<i>Canis mesomelas</i>	149.53	118.19	135.74
<i>Chrysocyon brachyurus</i>	136.44	123.63	148.50
<i>Cuon alpinus</i>	146.68	115.65	135.49
<i>Lycaon pictus</i>	138.51	117.91	142.47
<i>Nyctereutes procyonoides</i>	158.17	133.63	154.28
<i>Otocyon megalotis</i>	146.87	130.61	149.66
<i>Speothos venaticus</i>	119.11	107.42	132.87
<i>Vulpes corsac</i>	149.43	117.97	140.47
<i>Vulpes vulpes</i>	142.07	120.98	142.52
<i>Vulpes zerda</i>	137.66	122.45	148.10

Table 7. Temporalis lines of action

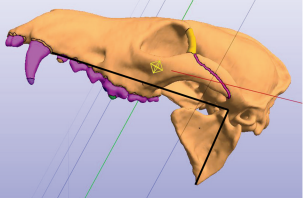
1A



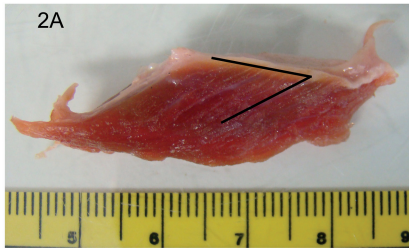
1B



1C



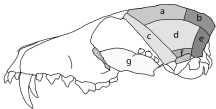
2A



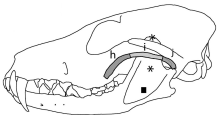
2B



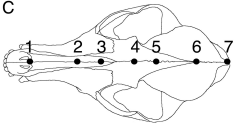
A



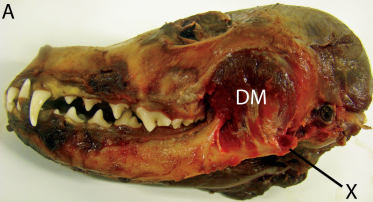
B



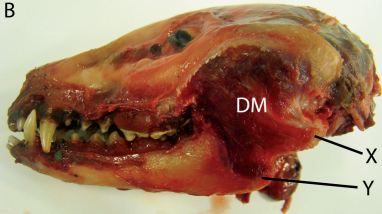
C

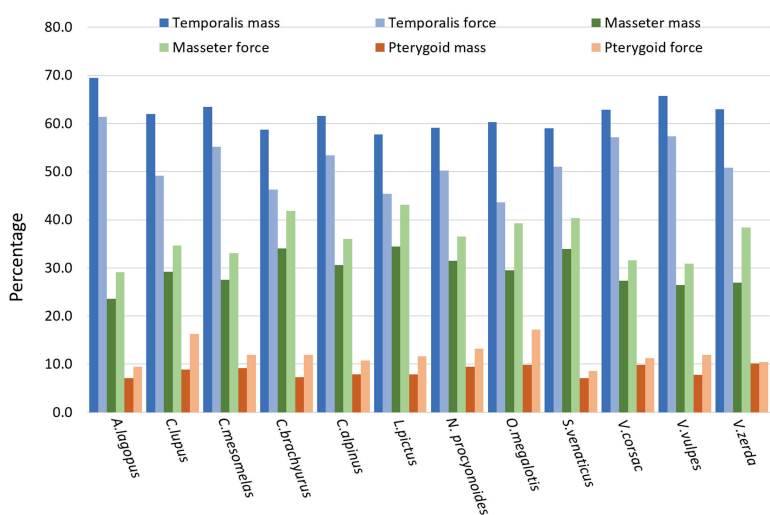


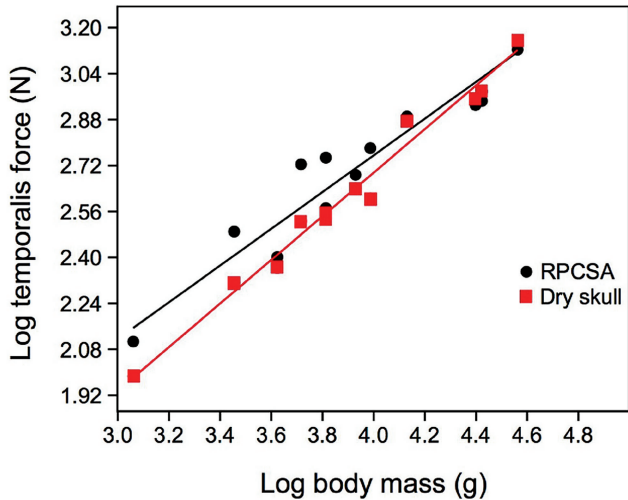
A

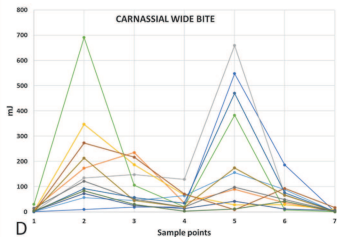
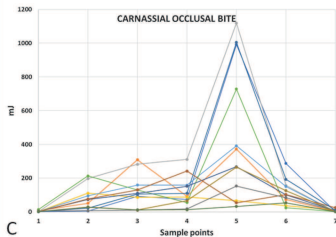
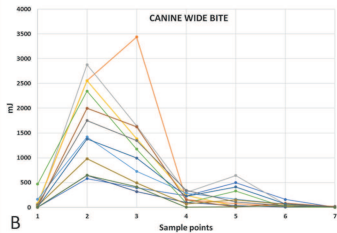
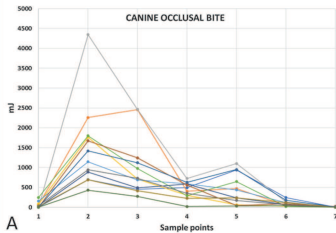


B









— *Alopex lagopus*

— *Canis lupus*

— *Canis mesomelas*

— *Chrysocyon brachyurus*

— *Cuon alpinus*

— *Lycaon pictus*

— *Nyctereutes procyonoides*

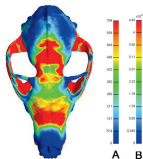
— *Otocyon megalotis*

— *Speothos venaticus*

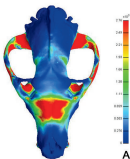
— *Vulpes corsac*

— *Vulpes vulpes*

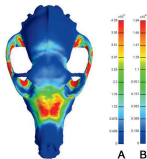
— *Vulpes zerra*



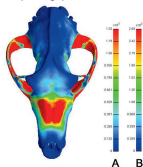
Alopex lagopus



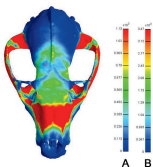
Canis lupus



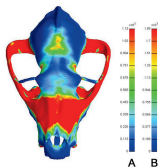
Canis mesomelas



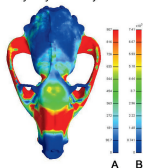
Chrysocyon brachyurus



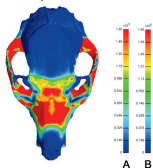
Cuon alpinus



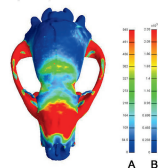
Lycaon pictus



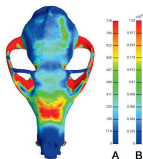
Nyctereutes procyonoides



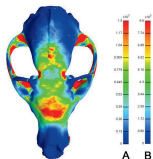
Otocyon megalotis



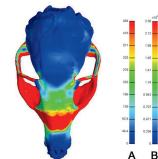
Speothos venaticus



Vulpes corsac

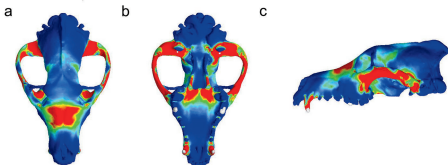


Vulpes vulpes

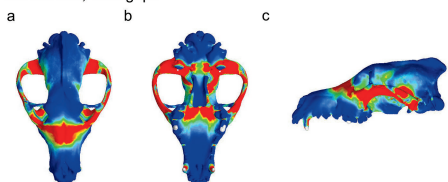


Vulpes zerda

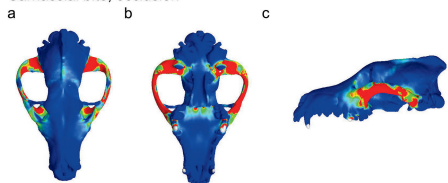
Canine bite, occlusion



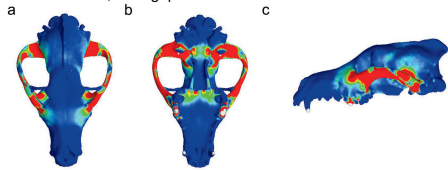
Canine bite, wide gape



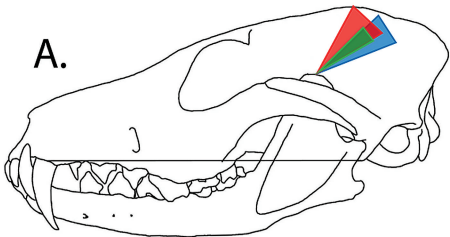
Carnassial bite, occlusion



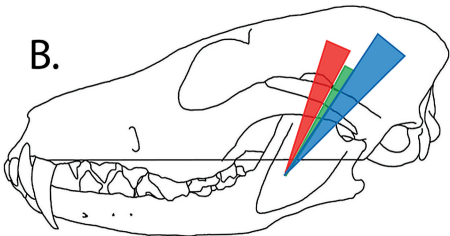
Carnassial bite, wide gape



A.



B.



C.

